

# Non-Identical Diffusion Models in MIMO-OFDM Channel Generation

Yuzhi Yang, Omar Alhussein, and Mérouane Debbah

KU 6G Research Center, College of Computing and Mathematical Sciences, Khalifa University, Abu Dhabi, UAE

E-mails: {yuzhi.yang, omar.alhussein, merouane.debbah}@ku.ac.ae

**Abstract**—We propose a novel diffusion model, termed the non-identical diffusion model, and investigate its application to wireless orthogonal frequency division multiplexing (OFDM) channel generation. Unlike the standard diffusion model that uses a scalar-valued time index to represent the global noise level, we extend this notion to an element-wise time indicator to capture local error variations more accurately. Non-identical diffusion enables us to characterize the reliability of each element (e.g., subcarriers in OFDM) within the noisy input, leading to improved generation results when the initialization is biased. Specifically, we focus on the recovery of wireless multi-input multi-output (MIMO) OFDM channel matrices, where the initial channel estimates exhibit highly uneven reliability across elements due to the pilot scheme. Conventional time embeddings, which assume uniform noise progression, fail to capture such variability across pilot schemes and noise levels. We introduce a matrix that matches the input size to control element-wise noise progression. Following a similar diffusion procedure to existing methods, we show the correctness and effectiveness of the proposed non-identical diffusion scheme both theoretically and numerically. For MIMO-OFDM channel generation, we propose a dimension-wise time embedding strategy. We also develop and evaluate multiple training and generation methods and compare them through numerical experiments.

**Index Terms**—Channel Estimation, Diffusion Model, MIMO, OFDM, Time Embedding

## I. INTRODUCTION

### A. Motivation and Related Works

In recent years, diffusion models have achieved great success in generation tasks [1], [2], and they have been widely applied in various fields [1]–[7]. In a typical diffusion noise-adding system, Gaussian white noise is gradually added to the target, whereas in the corresponding generation procedure, we gradually remove the noise to perform an inverse process of noise addition. Although generating from pure noise often leads to good results that follow the dataset distribution, it may be problematic in that we are not controlling the generation direction. Thus, it is also common to generate from coarse or imperfect estimations when a specific target output is desired.

When initializing the generation from rough estimations, we usually initialize the current time in the diffusion procedure based on the predicted distance between the initial value and the target. As frequently discussed in the overviews [8], [9], we can denoise [1], [2], fulfill [10]–[12], or edit [13]–[15] input images to generate outputs that satisfy task requirements through diffusion models. In the reconstruction of radio maps, there are also numerous works that generate radio maps from samples [16], [17] or past estimations [18].

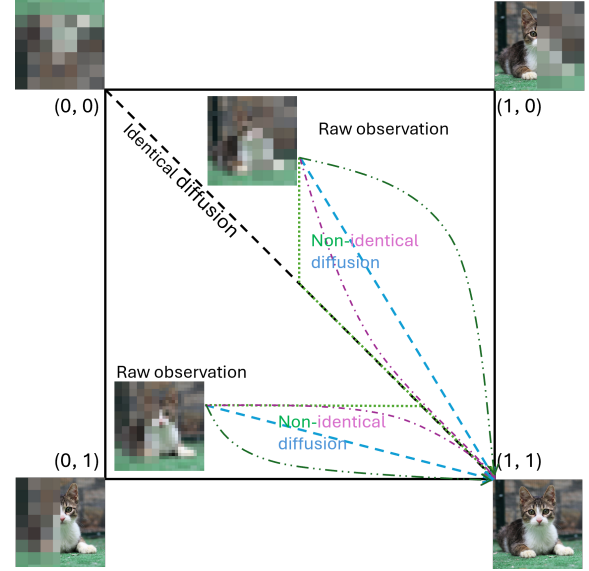


Fig. 1: A conceptual illustration of non-identical diffusion.

Extending this idea to wireless transceivers, similar generation problems from rough initializations are widespread. Unlike traditional neural network (NN)-based mapping frameworks, generative methods are gaining increased attention due to their high resilience to the ubiquitous noise in wireless systems [19]–[21]. Instead of generating solely from white noise, diffusion can be guided by initial imperfect MIMO channel estimates, enabling more targeted and accurate reconstruction [7], [22]. Further considering the orthogonal frequency division multiplexing (OFDM) scheme, prior work has shown that initializing the diffusion process with imperfect MIMO channel estimates can improve reconstruction quality [6], [23], which aligns with our approach. In addition, prior knowledge of data symbol distributions can be leveraged to guide the diffusion process and enhance the quality of the generated channel matrices [24], [25].

However, the initialization methods above consider all elements of the diffusion variable as having the same reliability, which is not accurate in some applications such as the wireless multi-antenna OFDM receiver. Some existing works obtain good results despite not taking into account that elements exhibit non-identical noise distribution [10]–[14], [23], [25]. Thus, there is a need for new diffusion methods where the time step in the diffusion procedure can be described accurately. As illustrated in Fig. 1, we show a typical diffusion procedure of a

cat image. Traditional diffusion model works focus on how to generate the right-bottom figure from the left-up noisy image, and the procedure follows the corresponding diagonal line. However, in many scenarios, we can have initial observations anywhere in the square. In this paper, we focus on such non-identical initializations, and investigate the diffusion procedure through different paths as shown in Fig. 1.

Specifically, in diffusion models, we typically use a time embedding that corresponds to a scalar value representing the overall noise level of the noisy input. However, the reliabilities of different elements in the original estimation often vary significantly. For example, those corresponding to pilots are always far more reliable than others. Thus, it is more ideal to represent the element reliabilities with a matrix. With element-wise representation, we can achieve more accurate descriptions of the diffusion procedure. In this paper, we investigate the diffusion model with non-identical time for each element, namely non-identical diffusion, and show its application in the MIMO-OFDM channel generation problem. In particular, we focus on the channel recovery task by initializing the diffusion process with an imperfect estimate characterized by a non-identical noise distribution across elements. Our approach is compatible with NN architectures proposed in prior diffusion-based works [1]–[4], [7].

One main challenge of non-identical diffusion models lies in the embedding method. Time embedding plays an essential role in traditional diffusion models, where the scalar time input is embedded to match the size of the input variables. However, such a method cannot be directly applied to non-identical diffusion models where the original time matrix already has the same size as the input. In MIMO-OFDM systems, resources are typically allocated by time slots, antennas, or subcarriers, and existing works have proven that we can use dimension-wise NN architectures in channel-related tasks [26]. Considering the dimension-wise structure, we further propose a column- and row-wise time embedding method for non-identical diffusion and investigate the impact of the training method, diffusion procedure, and initial distribution.

## B. Contributions

The contributions of this paper are summarized as follows:

- We propose the non-identical diffusion model, formally define its structure, and establish its theoretical correctness and relationship to standard diffusion models.
- We propose an interleaved time embedding method tailored for non-identical diffusion. When applied to the multi-antenna OFDM channel generation task based on multi-layer perceptron (MLP)-Mixer backbone, the proposed scheme outperforms the traditional diffusion scheme.
- We provide numerical evaluations to validate the proposed framework and analyze the effects of the noise injection strategy during training, the initialization pattern, and the time propagation scheme during generation.

## C. Notations

In this paper, non-bold symbols denote scalars or functions whose outputs are scalars. Bold italic lowercase letters represent vectors or functions whose outputs are vectors. Bold italic uppercase letters denote vector-valued random variables corresponding to the respective lowercase letters. Bold uppercase letters denote matrices. The operator  $\circ$  denotes the Hadamard product, and all scalar functions applied to vectors are to be understood as element-wise operations. Without loss of generality, although diffusion variables are complex-valued matrices in the application, they are represented as real vectors of length  $d$  for algorithmic presentation. Additionally,  $\|\cdot\|_2$  denotes the  $\ell$ -2 norm of a vector.  $\mathcal{R}$  and  $\mathcal{C}$  denote the sets of real and complex numbers, respectively.  $\mathbb{E}$  denotes expectation.  $\mathbf{0}$  and  $\mathbf{1}$  represent all-zero and all-one vectors, respectively, and  $\mathbb{I}$  denotes the identity matrix.

## II. NON-IDENTICAL DIFFUSION PROCESS

In this section, we give the definition of the proposed non-identical diffusion process. Throughout this paper, we refer to the traditional diffusion model as “identical diffusion model.” Although the diffusion variable is usually a matrix, we use its vectorized form when discussing the diffusion process.

### A. Noise adding process

Similar to the identical diffusion process [1], we define the non-identical diffusion process as follows:

**Definition 1.** A random process involving variable  $\mathbf{h} \in \mathcal{R}^d$  and time  $t \in [0, T)$  is called a non-identical diffusion process if it satisfies all the following conditions:

- 1)  $\alpha_t : [0, T) \rightarrow (0, 1]^d$  is a derivable non-increasing function such that  $\alpha_{t_1} \preceq \alpha_{t_2}$  for any  $t_1 > t_2$ .
- 2)  $\alpha_0 = \mathbf{1}$  and  $\lim_{t \rightarrow T} \alpha_t = \mathbf{0}$ .
- 3)  $\mathbf{H}_0 \sim \mu$ , which is the distribution of the dataset.
- 4) With  $\mathbf{W}_t$  representing the  $d$ -dimensional standard Brownian motion, the following Itô stochastic differential equation (SDE) holds:

$$d\mathbf{H}_t = [\log \alpha_t]' \circ \mathbf{H}_t dt + \sqrt{-2[\log \alpha_t]'} \circ d\mathbf{W}_t. \quad (1)$$

From Definition 1, we can prove the following probability measure flow, which is a trivial expansion of identical diffusion.

**Theorem 1.** The law of  $\mathbf{H}_t$  in Definition 1 is the same as that of  $\alpha_t \circ \mathbf{H}_0 + \beta_t \circ \xi$ , where  $\beta_t := \sqrt{1 - \alpha_t^2}$ , and  $\xi \sim \mathcal{N}(\mathbf{0}, \mathbb{I})$  is independent of  $\mathbf{H}_0$ , i.e., the PDF of  $\mathbf{H}_t$  is

$$\phi_t^\alpha(\mathbf{h}) = \int_{\mathcal{R}^d} \rho_{\beta_t}(\mathbf{h} - \alpha_t \circ \varepsilon) \mu(\varepsilon) d\varepsilon. \quad (2)$$

*Proof.* It is easy to verify the result. Due to the page limit, we provide a high-level outline of the proof. We can first use the Kolmogorov forward equation theorem to transform the Itô SDE in (1) to a Fokker-Planck PDE, and it is trivial to verify that the PDF of  $\alpha_t \circ \mathbf{H}_0 + \beta_t \circ \xi$  follows the Fokker-Planck PDE.

We also provide an intuitive understanding of this theorem. With a small positive  $\Delta t$ , we can approximate (1) as

$$\mathbf{H}_t - \mathbf{H}_{t-\Delta t} = \frac{\alpha_t - \alpha_{t-\Delta t}}{\alpha_{t-\Delta t}} \circ \mathbf{H}_{t-\Delta t} + \sqrt{\frac{\alpha_{t-\Delta t}^2 - \alpha_t^2}{\alpha_{t-\Delta t}^2}} \circ \boldsymbol{\xi}. \quad (3)$$

Thus,

$$\mathbf{H}_t = \frac{\alpha_t}{\alpha_{t-\Delta t}} \circ \mathbf{H}_{t-\Delta t} + \sqrt{1 - \left(\frac{\alpha_t}{\alpha_{t-\Delta t}}\right)^2} \circ \boldsymbol{\xi}, \quad (4)$$

which is a typical diffusion process.  $\square$

### B. Denoising process

Similar to the denoising diffusion implicit models (DDIM) algorithm in identical diffusion, we have the following ODE and theorem, showing a typical non-identical DDIM process.

$$d\mathbf{G}_t/dt = [\log \alpha_{T-t}]' \circ (\mathbf{G}_t - \mathcal{D}_{T-t}^\alpha(\mathbf{G}_t)) := b_t^\alpha(\mathbf{G}_t), \quad (5)$$

where

$$\mathcal{D}_t^\alpha(\mathbf{h}) := \mathbb{E}(\mathbf{H}_0 | \alpha_t \circ \mathbf{H}_0 + \beta_t \circ \boldsymbol{\xi} = \mathbf{h}). \quad (6)$$

**Theorem 2. (Correctness of non-identical DDIM)** Consider ODE (5) under the restrictions in Definition 1. Assume that  $\mu$  is bounded and has compact support. With any  $\alpha_t$  satisfying the requirements in Definition 1 and any starting point  $t_0$ , if  $\mathbf{G}_{t_0} \sim \phi_{T-t_0}^\alpha(\mathbf{g})$ , we have

$$\mathbf{G}_t \sim \phi_{T-t}^\alpha(\mathbf{g}), \forall t \in [t_0, T], \quad (7)$$

and thus  $\mathbf{G}_T \sim \mu$ . Therefore, for any initialization and any given path under the requirements in Definition 1, the inverse generation result always follows the original distribution of the dataset.

*Proof.* See Appendix A.  $\square$

Correspondingly, substituting differentials with differences in (5), we have the following vanilla non-identical DDIM algorithm.

$$\mathbf{g}^{\text{next}} = [\alpha^{\text{next}} - \alpha \circ \beta^{\text{next}} \circ \beta^{-1}] \circ \mathcal{D}^\alpha(\mathbf{g}) + \beta^{\text{next}} \circ \beta^{-1} \circ \mathbf{g}, \quad (8)$$

which can be directly obtained by substituting the derivation in (5) by differentiation. Furthermore, as suggested in the DDIM paper [2], we actually use the following hybrid version of DDPM and DDIM for better generation.

$$\mathbf{g}^{\text{next}} = [\alpha^{\text{next}} - \varepsilon \alpha \circ \beta^{\text{next}} \circ \beta^{-1}] \circ \mathcal{D}^\alpha(\mathbf{g}) + \varepsilon \beta^{\text{next}} \circ \beta^{-1} \circ \mathbf{g} + \sqrt{1 - \varepsilon^2} \beta^{\text{next}} \circ \boldsymbol{\xi}, \quad (9)$$

where the subscripts indicating time  $t$  are omitted,  $\boldsymbol{\xi}$  is an independently generated standard Gaussian noise and  $\varepsilon$  is any constant between 0 and 1.

The results in this section reveal that, when applying non-identical DDIM algorithms, all reasonable  $\alpha_t$ s approximately lead to the same distribution given the same starting point. Moreover, we do not necessarily cover all the generation paths in the training phase. Instead, covering all the high-frequency  $\alpha_t$  values during training is necessary when designing the training algorithm.

The error occurs due to the approximation error between the NN and the expectation, as well as the error introduced by replacing differentials with differences. The second item relies on the original data distribution  $\mu$ , which is hard to analyze quantitatively. However, similar problems have been well studied in designing the generation steps of identical diffusion models, and these can be directly extended to the non-identical case. The unique challenge introduced by non-identity arises from the NN's approximation error. The error behavior of the NN depends on both the noise power and the pattern. By choosing different paths for  $\alpha_t$ , we are effectively determining the evolution of the noise pattern. Even if the starting and ending points are fixed, we can still benefit from selecting an appropriate path. However, this problem is also infeasible to analyze quantitatively, and is therefore discussed in the simulation section of this paper.

## III. REALIZING NON-IDENTICAL DIFFUSION WITH NN

In this section, we introduce the NN used for non-identical diffusion models, and we provide the training and generation algorithm. As is well known in identical diffusion models, the NN is used to fit  $\mathcal{D}_t^\alpha(\mathbf{h})$ . We also note that the NN fitting can be indirect, such as using the velocity parameterization method [27], [28].

### A. Training

For the stability of NNs, we usually normalize the input before feeding it into the NN. In identical diffusion, we typically use  $\tilde{\mathbf{h}} := \sqrt{d}\mathbf{h}/\|\mathbf{h}\|_2$  instead of  $\mathbf{h}$  as the variable in diffusion, where  $\mathbf{h}$  represents the raw data from the dataset. However, in wireless scenarios, we can use  $\tilde{\mathbf{h}} := \sqrt{d}\mathbf{h}/\|\mathbf{h}\|_2$  instead, for better stability, since  $\|\mathbf{h}\|_2$  can always be accurately estimated through the power of the received signal, as indicated in [25].

However, in non-identical diffusion methods, since we do not necessarily need to directly use the variable in diffusion as the NN's input, whether to highlight the more reliable elements becomes a new problem. Specifically, we consider the following two different methods of representing  $\tilde{\mathbf{h}}_t = \alpha_t \circ \mathbf{h}_0 + \beta_t \circ \boldsymbol{\xi}$  for the NN input  $\hat{\mathbf{h}}_t$ :

- **Identical Total Power:** Here, we normalize the total power including original sample and the added noise of the input, that is,  $\hat{\mathbf{h}}_t := \tilde{\mathbf{h}}_t$ .
- **Identical Noise Power:** To highlight the more reliable elements, we can also normalize the power of the added noise. That is,  $\hat{\mathbf{h}}_t := Z\beta_t^{-1} \circ \tilde{\mathbf{h}}_t$ , where  $Z$  is the normalize factor to ensure  $\|\hat{\mathbf{h}}_t\|_2^2 = d$ . Recalling that  $\alpha^2 + \beta^2 = 1$ , by simple calculations we know  $Z = \sqrt{d}\|\beta_t^{-1}\|_2^{-1}$ .

Before completing the training algorithm, we still need to determine the choice of  $\alpha_t$  during training, which is essential and can severely affect performance. Unlike identical diffusion models, where we only have one diffusion path, we use a group of  $\alpha_t$  paths in non-identical diffusion models for generality. Intuitively, the selection of representative  $\alpha_t$ s should sufficiently cover the noise patterns used in generation to ensure successful results. Moreover, since we do not actually care about the entire diffusion process while adding noise, we only

---

**Algorithm 1: Non-Identical Diffusion Model Training**  
 (Velocity Parameterization)
 

---

**Input:** Initialized NN  $f(\mathbf{h}, \boldsymbol{\tau}; \boldsymbol{\theta})$ , batch size  $B$ , learning rate  $\eta$ , maximum time step  $T$ , sampling method of  $\boldsymbol{\tau}$

**while** not converged **do**

Sample  $\{\mathbf{h}_1, \dots, \mathbf{h}_B\}$  from the dataset;

Independently sample  $\{\boldsymbol{\tau}_1, \dots, \boldsymbol{\tau}_B\}$ ;

Independently sample  $\{\boldsymbol{\xi}_1, \dots, \boldsymbol{\xi}_B\}$  from standard Gaussian distribution with the same shape as  $\mathbf{h}$ ;

$\boldsymbol{\alpha}_i \leftarrow \gamma(\boldsymbol{\tau}_i)$ , where  $\gamma$  is defined in (10);

$\boldsymbol{\beta}_i \leftarrow \sqrt{1 - \boldsymbol{\alpha}_i^2}$ ,  $\hat{\mathbf{h}}_i \leftarrow \boldsymbol{\alpha}_i \circ \mathbf{h}_i + \boldsymbol{\beta}_i \boldsymbol{\xi}_i$ ;

**if** using identical noise power **then**

$\hat{\mathbf{h}}_i \leftarrow \sqrt{d} \|\boldsymbol{\beta}_i^{-1}\|^{-1} \boldsymbol{\beta}_i^{-1} \circ \hat{\mathbf{h}}_i$ ;

**end if**

$\mathbf{y}_i \leftarrow \boldsymbol{\alpha}_i \circ \boldsymbol{\xi}_i - \boldsymbol{\beta}_i \circ \mathbf{h}_i$  (Velocity Parameterization);

$\ell \leftarrow \sum_{i=1}^B \|f(\hat{\mathbf{h}}_i, \boldsymbol{\tau}; \boldsymbol{\theta}) - \mathbf{y}_i\|_2^2$ ;

$\boldsymbol{\theta} \leftarrow \boldsymbol{\theta} - \eta \partial \ell / \partial \boldsymbol{\theta}$ ;

**end while**

---

need to focus on the distribution of all  $\boldsymbol{\alpha}_t$ s when randomly selecting  $\boldsymbol{\alpha}$  and  $t$ .

To simplify this procedure, we use a non-increasing unary function  $\gamma : [0, T] \rightarrow (0, 1]$ , such that  $\gamma(0) = 1$ ,  $\lim_{\tau \rightarrow T} \gamma(\tau) = 0$ , and  $\gamma(\boldsymbol{\tau})$  follows the same distribution as  $\boldsymbol{\alpha}_t$ . We note that the function  $\gamma$  can be directly introduced from the common function  $\alpha$  in identical diffusion models, where vector  $\boldsymbol{\tau}$  plays the non-identical part. Therefore, we can use the following  $\gamma$  function for integer inputs with the common hyperparameter setting [1] and define different noise patterns by selecting  $\boldsymbol{\tau}$ .

$$\gamma(\tau) := \prod_{i=1}^{\tau} \sqrt{1 - 0.2i/T}. \quad (10)$$

Specifically, in this paper, we consider the following straightforward noise patterns defined through  $\boldsymbol{\tau}$ .

- **Same:** A method to imitate identical diffusion, where  $\boldsymbol{\tau} = x\mathbf{1}$  and  $x$  are uniformly drawn from  $\{0, \dots, T-1\}$ .
- **Independent:** Another straightforward method where each element in  $\boldsymbol{\tau}$  are independently and uniformly drawn from  $\{0, \dots, T-1\}$ .
- **Pattern-Independent:** A method between same and completely independently drawing. Since the dimension  $d$  is usually very large in practice, completely independent drawing becomes inefficient. By exploring the patterns in the potential initialization for generation, we can only draw a small set of  $\boldsymbol{\tau}$  randomly and then complete it with some given pattern. In this paper, we use recurrent patterns since we usually insert pilots recurrently in OFDM systems.
- **Mixed:** For better generality, we can use a mixed method where we randomly choose noise patterns generated from the methods above.

---

**Algorithm 2: Non-Identical Diffusion Generation**


---

**Input:** Trained NN  $f(\mathbf{h}, \boldsymbol{\tau}; \boldsymbol{\theta})$ , initial estimation  $\tilde{\mathbf{h}}^{(0)}$ , initial time indicator  $\boldsymbol{\tau}^{(0)}$ , total generation steps  $N_G$

$\mathbf{g} \leftarrow \tilde{\mathbf{h}}^{(0)}$ ,  $\boldsymbol{\tau} \leftarrow \boldsymbol{\tau}^{(0)}$ ;

$\boldsymbol{\alpha} \leftarrow \gamma(\boldsymbol{\tau})$ ,  $\boldsymbol{\beta} \leftarrow \sqrt{1 - \boldsymbol{\alpha} \circ \boldsymbol{\alpha}}$ , where  $\gamma$  is defined in (10);

**while**  $\boldsymbol{\tau}$  is not zero **do**

Calculate  $\boldsymbol{\tau}^{\text{next}}$  by (13);

$\boldsymbol{\alpha}^{\text{next}} \leftarrow \gamma(\boldsymbol{\tau}^{\text{next}})$ ,  $\boldsymbol{\beta}^{\text{next}} \leftarrow \sqrt{1 - \boldsymbol{\alpha}^{\text{next}} \circ \boldsymbol{\alpha}^{\text{next}}}$ ;

**if** using identical noise power **then**

$\mathbf{g} \leftarrow \sqrt{d} \|\boldsymbol{\beta}^{-1}\|^{-1} \boldsymbol{\beta}^{-1} \circ \mathbf{g}$ ;

**end if**

$D^\alpha(\mathbf{g}) \leftarrow \boldsymbol{\alpha} \circ \mathbf{g} - \boldsymbol{\beta} \circ f(\mathbf{g}, \boldsymbol{\tau}; \boldsymbol{\theta})$  (Velocity Parameterization);

Calculate  $\mathbf{g}^{\text{next}}$  by (9);

$\mathbf{g} \leftarrow \mathbf{g}^{\text{next}}$ ,  $\boldsymbol{\tau} \leftarrow \boldsymbol{\tau}^{\text{next}}$ ,  $\boldsymbol{\alpha} \leftarrow \boldsymbol{\alpha}^{\text{next}}$ ;

**end while**

Output  $\hat{\mathbf{h}} \leftarrow \mathbf{g}$  as final generation.

---

Further, we denote the NN as  $f(\mathbf{h}, \boldsymbol{\tau}; \boldsymbol{\theta})$ , where  $\boldsymbol{\theta}$  is the parameter and take velocity parameterization [27], [28] as an example. Thus, the target of the NN becomes

$$\min_{\boldsymbol{\theta}} \text{KL} \left( f(\mathbf{H}, \boldsymbol{\tau}; \boldsymbol{\theta}) \| \gamma(\boldsymbol{\tau}) \circ \boldsymbol{\xi} - \sqrt{1 - \gamma^2(\boldsymbol{\tau})} \circ \tilde{\mathbf{h}}_0 \right), \quad (11)$$

where  $\text{KL}(\cdot \| \cdot)$  denotes the Kullback-Leibler Divergence. Furthermore, by variational inference, we can define the loss function as

$$\ell = \sum_{i=1}^B \|f(\hat{\mathbf{h}}_i, \boldsymbol{\tau}; \boldsymbol{\theta}) - \mathbf{y}_i\|_2^2, \quad (12)$$

where  $\mathbf{y}_i := \gamma(\boldsymbol{\tau}_i) \circ \boldsymbol{\xi}_i - \sqrt{1 - \gamma^2(\boldsymbol{\tau}_i)} \circ \hat{\mathbf{h}}_i$ .

### B. Generation

A typical generation procedure mainly follows (9). More specifically, we take the velocity parameterization as an example and show the generation procedure of one sample in Algorithm 2. However, as in the original DDIM algorithm, the time flow in generation does not necessarily need to be the same as in training. Especially when the initial time is non-identical, we generally have two generation strategies: uniform stepping and water-filling.

As described above, we use the same unary function  $\gamma$  to map non-identical  $\boldsymbol{\tau}$  to  $\boldsymbol{\alpha}_t$ . Again, since we usually care about the  $\boldsymbol{\alpha}$  value after each step rather than the diffusion procedure itself (as in common identical DDIM systems), we focus on the evolution of  $\boldsymbol{\tau}$  instead. Specifically, we denote  $\boldsymbol{\tau}_0$  as the initial value obtained from the estimation algorithm, and  $N_G$  as the total number of generation steps.

The uniform stepping method is straightforward where we reduce the time uniformly so that  $\boldsymbol{\tau}^{\text{next}} = \boldsymbol{\tau} - \boldsymbol{\tau}_0/N_G$ , where  $N_r$  stands for the number of remaining steps. Another straightforward method is to first improve the worse elements to the reliability of the better ones, and then proceed as in the identical DDIM, i.e., the water-filling algorithm. That

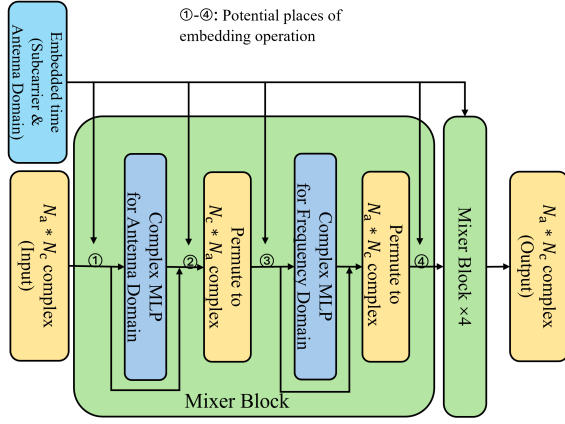


**Fig. 2:** The backbone NN structure used in this paper, where ①-④ are potential places for time embedding operations.

is, we always try to find a  $\tau^{\text{next}}$  such that  $\tau^{\text{next}} \preceq \tau$ ,  $|\tau - \tau^{\text{next}}|_1 = |\tau_0|1/NG$ , and  $\tau_i^{\text{next}} \leq \tau_j^{\text{next}}$  always holds if  $\tau_i \leq \tau_j$ . In the following, we denote this procedure as  $\tau^{\text{next}} = \text{Waterfilling}(\tau, |\tau_0|1/NG)$ .

We can also define a hybrid stepping method as:

$$\tau^{\text{next}} = \epsilon(\tau - \tau_0/NG) + (1 - \epsilon)\text{Waterfilling}(\tau, |\tau_0|1/NG), \quad (13)$$

where  $\epsilon \in [0, 1]$ . This approach reduces to uniform stepping when  $\epsilon = 1$ , and to water-filling when  $\epsilon = 0$ , thereby completing Algorithm 2. Similarly, we can also define these stepping methods based on  $\alpha$  instead of  $\tau$ . The details of the velocity parameterization method [27], [28] are omitted here due to page limitations.

#### IV. NON-IDENTICAL TIME EMBEDDING FOR MULTI-ANTENNA OFDM CHANNELS

In this section, we tackle a technical problem: how to embed  $\tau$  into the NN. Unlike identical diffusion models, we have an independent time indicator for each element. However, common time embedding methods typically embed the scalar time into specific patterns, which cannot be directly applied to non-identical diffusion models. Thus, we propose to average the current  $\tau$  along each dimension, and perform embedding independently. We note that this section is specific to the Multi-Antenna OFDM channel reconstruction task, and may serve as a reference for the designs of time embedding modules in other non-identical diffusion tasks.

##### A. Problem Statement and Backbone NN

We consider a typical OFDM setting with a multi-antenna BS and a single-antenna UE. Thus, the channel can be denoted as  $\mathbf{H} \in \mathbb{C}^{N_a \times N_c}$ , where  $N_a$  and  $N_c$  denote the numbers of BS antennas and subcarriers, respectively. Our task is to recover this channel matrix from a partial and noisy initial observation. Specifically, we assume that we have an original estimation  $\bar{\mathbf{H}}$  of  $\mathbf{H}$  with a reliability map  $\mathbf{M} \succeq 0$ , such that

$$\bar{\mathbf{H}} - \mathbf{M} \circ \mathbf{H} \sim \mathcal{CN}(\mathbf{0}, \mathbb{I}), \quad (14)$$

which is a common assumption in channel estimation algorithms. We omit the details regarding the implementation of

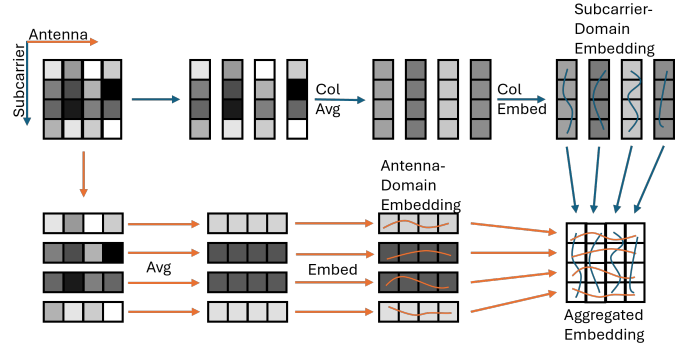


**Fig. 3:** A conceptual illustration of the proposed two-dimensional time embedding method

the system and the specific method of obtaining  $\bar{\mathbf{H}}$  and  $\mathbf{M}$ , treating them as originally provided inputs.

We note that although the channel here is a two-dimensional complex matrix instead of the real vectors discussed above, the difference only lies in the design of the backbone NN, and the algorithms described above can be directly applied.

Thus, corresponding to the non-uniform diffusion method above, we can rewrite the initialization as

$$\tilde{H}_{i,j}^{(0)} = \bar{H}_{i,j}/(M_{i,j} + 1), \quad (15)$$

$$\tau_{i,j}^{(0)} = \gamma^{-1}(M_{i,j}/(M_{i,j} + 1)), \quad (16)$$

which can be directly applied to Algorithm 2.

As for the backbone NN structure, we adopt the interleaved learning scheme based on MLP-Mixer, which has shown incredible performance in similar tasks [25], [26], [29]. Specifically, we adopt the exactly same backbone NN as in these works with different time embedding methods, which is also illustrated in Fig. 2.

##### B. Two-Dimensional Time Embedding

In non-identical diffusion models, conducting effective time embedding becomes a new problem. In identical diffusion models, we usually learn a mapping between unary time and patterns for embedding. However, in non-identical cases, each element corresponds to an independent time, making it impossible to generate a pattern for each element in the time matrix.

On the other hand, we note that in multi-antenna OFDM systems, the resource allocation is typically based on subcarriers or antennas, inspiring us to conduct time embedding per subcarrier and per antenna. By averaging along each dimension, the averaged result can maintain most of the original characteristics across almost all pilot schemes. Moreover, such a one-dimensional embedding structure can be easily incorporated into the interleaved learning scheme, as illustrated in Fig. 3.

In particular, in the interleaved learning scheme, we have two groups of modules dedicated to subcarriers and antennas, respectively. From the time embedding scheme, we can also generate two time embedding vectors corresponding to both

dimensions. Intuitively, we can use the following averaged time for embedding.

$$\tau_c^{(\text{time})} = \text{round}(\tau \mathbf{1}/N_c), \quad (17)$$

$$\tau_a^{(\text{time})} = \text{round}(\tau^T \mathbf{1}/N_a), \quad (18)$$

where  $\text{round}(\cdot)$  denotes the rounding function producing integer time for further processing. We note that  $\tau_c$  averages the time in different subcarriers and keeps each antenna independent. Therefore, it is called subcarrier-domain mapping. Similarly,  $\tau_a$  is called the antenna-domain mapping.

On the other hand, as the time in a diffusion model stands for the power ratio of the desired variable in the estimation, we can also average over  $\alpha$  for power-averaging.

$$\tau_c^{(\text{power})} = \text{round}(\gamma^{-1}(\gamma(\tau) \mathbf{1}/N_c)), \quad (19)$$

$$\tau_a^{(\text{power})} = \text{round}(\gamma^{-1}(\gamma(\tau)^T \mathbf{1}/N_a)), \quad (20)$$

Incorporating this with the interleaved learning framework, we have the following three embedding methods, which complete the NN design.

- **Row-Wise Embedding:** We perform time embedding along the same domain as the interleaved learning unit. That is, we apply the subcarrier-domain embedding  $\tau_a$  at points ① and ②, and  $\tau_c$  at ③ and ④ in Fig. 2, respectively.
- **Column-Wise Embedding:** We can also perform time embedding along different domain of the interleaved learning unit such that we apply  $\tau_a$  at points ③ and ④, and  $\tau_c$  at ② and ③ in Fig. 2, respectively.
- **Embedding Together:** We can also overlook the detailed structure of the interleaved learning and conduct both embedding integrally. That is, we apply both  $\tau_c$  and  $\tau_a$  at points ① and ④, and do nothing at ② and ③ in Fig. 2.

## V. NUMERICAL RESULTS

### A. Dataset and Basic Settings

Following the experimental settings in [25], we consider the multi-antenna OFDM scenario using the DeepMIMO [30] dataset. We use the same data preprocessing method as in [25]. The shape of the channel matrix  $\mathbf{H}$  is given by  $N_a = 32$ ,  $N_c = 64$ , corresponding to the number of BS antennas and OFDM symbols. The first subcarrier lies at 3.5 GHz, and the subcarrier spacing is 300 kHz. We have 43,440 channel matrices in the training dataset and 10,860 in the testing dataset. In the training phase, we only use the training dataset, while the testing dataset is exclusively used in the generation experiments. We note that we overlook the detailed communication scheme in this paper and only focus on how to generate high-quality channel matrices from partial, noisy initial observations.

### B. Training Results

In this section, we show the training results of the proposed non-identical diffusion model. Specifically, we conducted 48

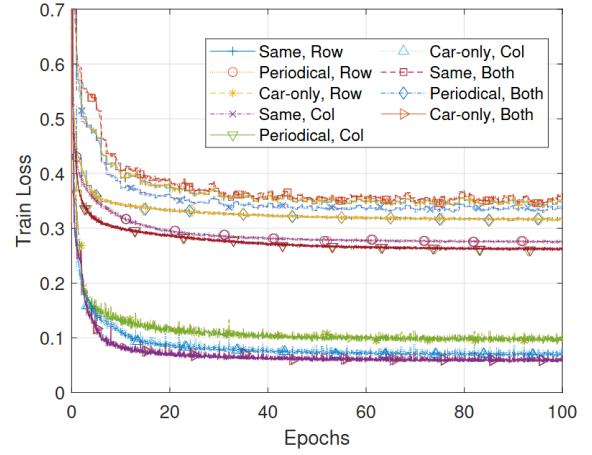


**Fig. 4:** Training convergence curve with different embedding methods.

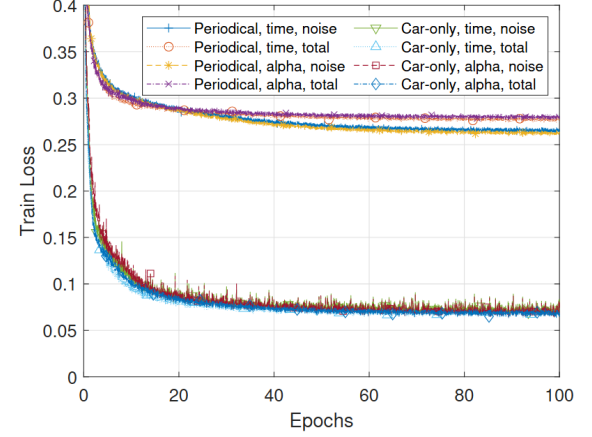


**Fig. 5:** Training convergence curve with different normalization and dimensional averaging methods.

independent training experiments corresponding to two representing methods of  $\mathbf{h}_i$  as explained in Section III A, three time embeddings, and two time averaging methods as introduced in Section IV B, and the following four noise patterns:

The “same” pattern as introduced in Section III A. The “independent” pattern also introduced in Section III A. The “periodical” pattern, where the noise matrices are periodic in both dimensions to imitate common pilot schemes. In particular, the period in the subcarrier domain is randomly and uniformly selected between 4 and 20, while that in the antenna domain is between 4 and 10. The “car-only” pattern, where the noise powers corresponding to each subcarrier are the same, while those of different subcarriers are independent, which is typical in uplink scenarios.

In the remainder of this section, we show some typical curves to compare different settings, and a complete result table of all 48 experiments can be found in Table I. In addition to the experiments above, we also conducted experiments on two mixed noise patterns: the “non-directional” pattern, where we uniformly and randomly choose from patterns 1–3 above; and the “all” pattern, where we uniformly and randomly choose from all simple patterns. In Table I, we focus on the training loss from epochs 51 to 100 after convergence and show the mean value and standard deviation for each



		Same		Independent		Periodical		Car-only	
		Identical noise	Identical power	Identical noise	Identical power	Identical noise	Identical power	Identical noise	Identical power
Row	$\tau$ avg	$0.346 \pm 0.024$	$0.334 \pm 0.022$	$0.274 \pm 0.001$	$0.275 \pm 0.001$	$0.233 \pm 0.009$	$0.264 \pm 0.006$	$0.094 \pm 0.002$	$0.089 \pm 0.002$
	$\alpha$ avg	$0.345 \pm 0.024$	$0.334 \pm 0.022$	$0.275 \pm 0.001$	$0.277 \pm 0.001$	$0.230 \pm 0.009$	$0.263 \pm 0.006$	$0.097 \pm 0.003$	$0.084 \pm 0.002$
Col	$\tau$ avg	$0.331 \pm 0.023$	$0.327 \pm 0.022$	$0.265 \pm 0.001$	$0.277 \pm 0.001$	$0.228 \pm 0.009$	$0.262 \pm 0.006$	$0.072 \pm 0.003$	$0.068 \pm 0.002$
	$\alpha$ avg	$0.334 \pm 0.023$	$0.327 \pm 0.022$	$0.262 \pm 0.001$	$0.280 \pm 0.001$	$0.222 \pm 0.008$	$0.258 \pm 0.007$	$0.070 \pm 0.003$	$0.068 \pm 0.002$
Both	$\tau$ avg	$0.338 \pm 0.024$	$0.318 \pm 0.023$	$0.326 \pm 0.001$	$0.259 \pm 0.001$	$0.232 \pm 0.007$	$0.248 \pm 0.006$	$0.062 \pm 0.002$	$0.057 \pm 0.001$
	$\alpha$ avg	$0.351 \pm 0.032$	$0.318 \pm 0.023$	$0.316 \pm 0.001$	$0.263 \pm 0.001$	$0.223 \pm 0.007$	$0.244 \pm 0.006$	$0.059 \pm 0.002$	$0.055 \pm 0.001$

**TABLE I:** Training loss (NMSE) after convergence under different non-identical training methods

independent experiment. We note that it is not fair to compare the results across different noise patterns. Instead, we only focus on comparisons within the same noise patterns here, and we evaluate different training noise patterns through the generation results.

We also show the convergence curves for some specific experiments in Figs. 4 and 5. In Fig. 4, we show the results under different time embedding methods with alpha-average sampling, and the input is normalized by identical noise power. In Fig. 5, we show the results with different normalization and dimensional averaging methods using column-wise time embedding. From Figs. 4, 5, and Table I, we have the following observations. Among different noise patterns, the “same” pattern shows remarkably worse performance, mainly due to the larger probability of extremely bad cases compared to other patterns. Also, the “car-only” pattern outperforms all other patterns since it is highly structural. However, such comparisons among different training noise patterns do not directly indicate the NN’s capability, since they are essentially different tasks. Thus, they need to be further evaluated through generation results.

The results of different embedding patterns show that column-wise embedding, where the NN layer and embedding vector operate on vertical dimensions, exhibits better performance. Such a phenomenon might be caused by the high variety of embedding patterns in the NN’s operational dimension, allowing it to focus on more reliable elements. The results of different normalization methods show that normalizing the total power leads to faster convergence but lower performance after convergence. An intuitive explanation is that normalizing the noise power can correctly highlight the more reliable part, which is exactly the main purpose of the time embedding layers. Thus, it shows better performance after convergence. However, the noise normalization method leads to unbalanced input power, which makes initial convergence more difficult. On the other hand, the averaging method shows marginal differences in performance, which need further investigation through generation results.

### C. Generation Results

1) *Generation Experiment Settings:* When evaluating the generation performance, we use the test set of the aforementioned dataset. Specifically, we apply  $N_G = 50$  steps of non-identical DDIM generation with  $\varepsilon = 0.4$ . Within each experiment, we use the same noise pattern for the initial channel estimation. Specifically, we use the following noise initializations, which are also illustrated in Fig. 6. We first allocate 10% of the total noise energy evenly among all elements as background noise. The remaining 90% is generated

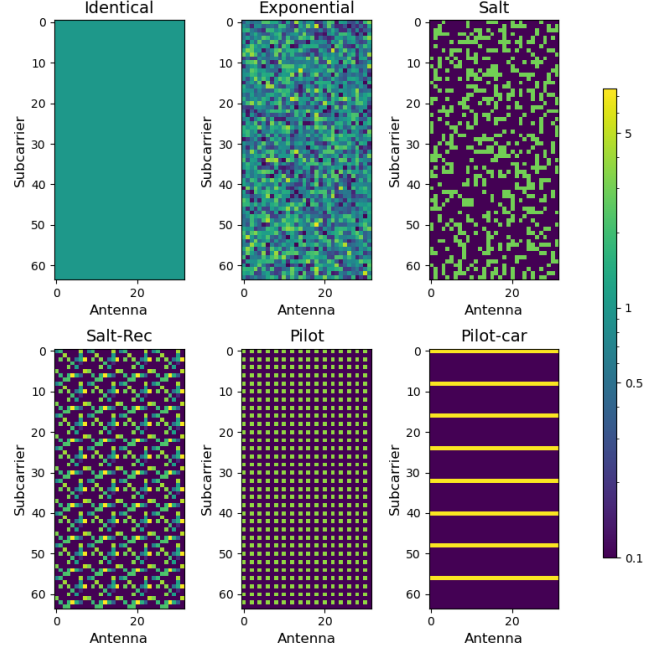


**Fig. 6:** An illustration of different initial noise patterns. The noise power are normalized and only the power is shown.

from one of the following distributions, completing the power map. The noise is independently Gaussian-distributed with the generated power map. We note that when using masked inputs, the following noises are only applied to the remaining elements.

- **White:** As a benchmark method, the power is identical among all elements, i.e., Gaussian white noise. The default signal-to-noise ratio (SNR) is -10 dB.
- **Exponential (Exp):** The noise power of each element independently follows an exponential distribution with a rate of 0.5. The default SNR is -5 dB.
- **Salt:** We apply a randomly generated mask retaining 30% of the elements. The power is identical among all remaining elements. The default SNR is 0 dB.
- **Salt-Rec:** The noise map is generated recurrently every 8 antennas and 8 subcarriers. Within each section, a mask retains 30% of the elements, and the noise power is exponentially distributed with a rate of 0.5. Such a noise map is representative of actual pilot schemes, which are typically recurrent. The default SNR is 0 dB.
- **Pilot:** We use a typical recurrent pilot scheme where the spacing is 2 in both antennas and subcarriers. The power is identical among all remaining elements. The default SNR is 10 dB.
- **Pilot-Car:** In some applications like uplink transmission,

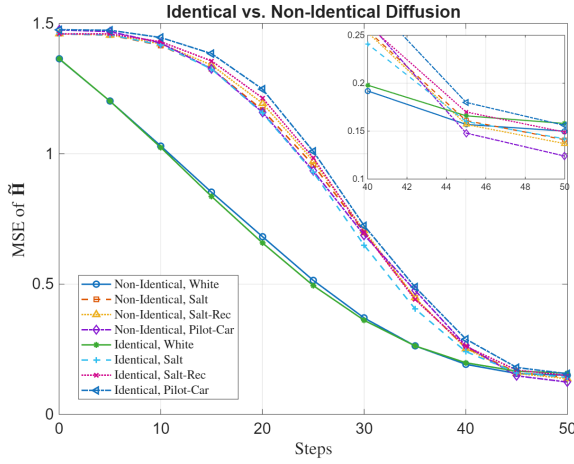


Fig. 7: The comparison between identical and non-identical diffusion models.

Initialization	Exp	Salt	Salt-Rec	Pilot	Pilot-Car
$\tau$ -Linear	0.098	0.202	0.172	0.386	0.276
$\tau$ -Hybrid (0.7)	0.095	0.189	0.155	0.367	0.225
$\tau$ -Hybrid (0.5)	0.094	0.182	0.147	0.358	0.205
$\tau$ -Hybrid (0.3)	0.093	0.177	0.141	0.350	0.193
$\tau$ -Waterfilling	0.092	<b>0.170</b>	<b>0.135</b>	<b>0.342</b>	<b>0.187</b>
$\alpha$ -Linear	0.096	0.230	0.199	0.389	0.295
$\alpha$ -Hybrid (0.7)	0.093	0.213	0.177	0.373	0.231
$\alpha$ -Hybrid (0.5)	0.092	0.205	0.170	0.367	0.218
$\alpha$ -Hybrid (0.3)	0.091	0.199	0.164	0.363	0.214
$\alpha$ -Waterfilling	<b>0.090</b>	0.192	0.158	0.361	0.219

TABLE II: The last-step performance of different stepping methods under different initializations, where the numbers in blankets represent the value of  $\epsilon$  in (13).

all antennas are used simultaneously. Thus, we use another pilot setting where the period is 8 in subcarriers, and the antennas are either all masked or all retained for each subcarrier. The power is identical among all remaining elements. The default SNR is 10 dB.

2) *Comparison With Identical Diffusion*: In Fig. 7, we show the comparison between the proposed non-identical diffusion model and the traditional identical framework as in [25]. We use four kinds of noise initialization for generation and show the NMSE error of the diffusion variable, i.e., channel matrix  $\mathbf{H}$ , after each step. In the non-identical diffusion settings, we use column-wise embedding, averaging over  $\alpha$ , diffusion variables with normalized power, and a  $\tau$ -waterfilling scheduler, which is chosen based on prior experiments.

From Fig. 7, we can find that both types of diffusion models can successfully produce good generation results that follow similar diffusion procedures. It is intuitive since they can both be characterized by similar time flows. Further, we can evaluate them by the performance of the last steps, which is heavily determined by the backbone NN’s performance. The results show that the non-identical diffusion scheme remarkably outperforms the identical one under the “Pilot-Car” noise pattern, is slightly better under the “Salt-Rec” pattern, and has almost the same performance under “White” and “Salt” patterns. Such results are easy to understand: the more the noise distribution is biased from identical, the better non-identical diffusion models perform.

Training Noise	White	Exp	Salt	Salt-Rec	Pilot	Pilot-Car
Same	0.263	0.100	0.328	0.306	0.817	0.336
Independent	0.434	0.189	0.631	0.595	0.893	0.628
Periodical	0.299	0.177	0.339	0.284	0.495	0.297
Car-Only	1.028	0.715	1.076	0.950	1.069	0.928
Non-Directional	0.171	0.100	0.182	0.146	0.453	0.196
All	<b>0.156</b>	<b>0.092</b>	<b>0.170</b>	<b>0.135</b>	<b>0.342</b>	<b>0.187</b>

TABLE III: The performance of different training noise patterns under different initialization of generation.

3) *Impact of Stepping Method*: Table II shows the final generation results with different stepping methods. We use the column-wise embedding method with identical noise input and embedding based on  $\alpha$ , which performs best during training. For the sake of generalization, we use the NN trained under the “All” noise pattern. Comparing within each row, we observe that the waterfilling method based on time  $\tau$  outperforms all other stepping methods in most cases. This result is intuitive, since the NN usually works better when the noise distribution is more balanced, and existing works in identical diffusion models also show that stepping by  $\tau$  is superior to stepping by  $\alpha$ . We also used the trained model with identical power inputs for the same experiments, which also showed similar results and is omitted here due to page limits.

4) *Generating Performance Under Different Training Noise Patterns*: In this section, we investigate the effect of different training noise schemes, as shown in Table III. We inherit the basic settings above and use the  $\tau$ -Waterfilling method for stepping. As the noise pattern has a vital effect on the NN’s performance, aligning the noise-adding method during training with the initialization of generation becomes necessary. From Table III, we observe the following interesting findings. Like what we did above, we also repeated the experiments with the trained model having identical power inputs, showing similar results, and also omit them here.

First, the “same” noise pattern, indicating identical training noise power, performs surprisingly well compared with most specific training patterns, verifying the success of previous identical diffusion works. Especially when the initial noise does not contain much structural information, it performs almost the best. This is intuitive, since we cannot benefit much from the initial noise structure. Meanwhile, although the models trained under specific noise patterns seem to work well during training, they fail to obtain good generation results—even under a similar initial noise pattern—except for the periodic training noise pattern. A possible explanation for this phenomenon is as follows. It is hard to describe such distributions by sampling due to their complexity, while all samplings share the same pattern. Thus, the NN may focus on some biased knowledge instead of the dimension-wise noise embedding, resulting in degraded generalization performance. Although such special noise patterns cannot lead to a good training result independently, they can still greatly improve the generation capability by providing diverse and complementary training signals, as inferred from the results of hybrid training noise patterns.

5) *Impact of Embedding Schemes*: In Fig. 8, we reevaluate the impact of different embedding schemes as shown in Table



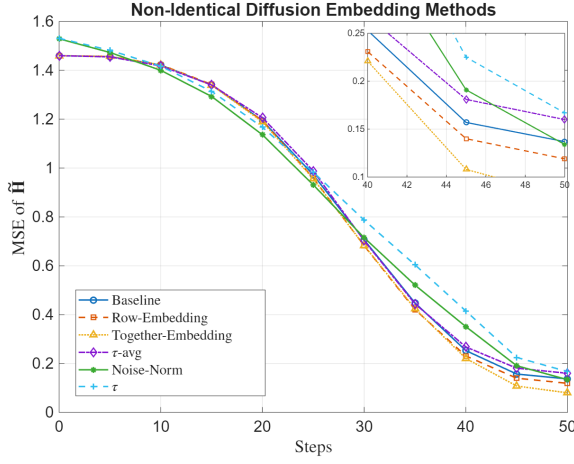


Fig. 8: The generation results of different embedding schemes.

I, where “baseline” indicates the column-embedding,  $\alpha$ -avg, power-normalization result, and other names indicate their minimum differences to the baseline. These results generally look similar to those in Table I. However, there are two main results that are worth pointing out: the methods with power-normalized inputs outperform those with noise-normalized inputs; and the good performances of the “Row” and “Together” embedding methods. These phenomena do not always occur when we change to other settings. Thus, we cannot find the explanation and remain them as an open problem.

## VI. CONCLUSION AND FUTURE DIRECTIONS

In this paper, we introduced the non-identical diffusion model, a generalization of traditional diffusion models that employs a matrix-based time representation to better capture element-wise noise distributions. This formulation is particularly effective when the initial confidence varies across elements. We derived the corresponding PDE formulation and extended the DDIM algorithm to support the non-identical diffusion setting. We also proposed alternative training methods and generation strategies. For the MIMO-OFDM channel generation task, we further proposed a dimension-wise time embedding scheme. Numerical results demonstrated the effectiveness of the proposed non-identical diffusion system and highlighted the advantages of the proposed methods across different configurations.

This paper mainly focused on the systematic design and proposed heuristic algorithms, leaving various directions for future work. One important direction is to further delve into the stepping methods. Our results showed that the waterfilling method usually outperforms other methods. Further efforts are needed to clarify whether this phenomenon also holds in other problems and if waterfilling indicates the optimal path in general non-identical diffusion models. Moreover, there seems to be a complicated interplay between the embedding schemes and training and generation performances, requiring further examination. In addition, the training method warrants further improvement, as our results indicate that the diversity of training data plays a critical role in generation performance.

For the MIMO-OFDM scenario examined, it is still essential to further combine the proposed methods with the actual resource block structures and signal modulations as in [25], [29].

The authors have provided public access to their code and more detailed results at: [https://anonymous.4open.science/r/Non-Identical\\_diffusion-9553](https://anonymous.4open.science/r/Non-Identical_diffusion-9553).

## APPENDIX A PROOF TO THEOREM 2

This proof mainly follows that of Theorem 2.8 in [31]. Since  $\mu$  has a compact support, following Lemma 2.6 in [31], we know that  $\mathcal{D}_t^\alpha$  is Lipschitz continuous and follows the linear growth condition. Thus, ODE (5) has a unique solution with any starting point  $G_{g_0}$ , which implies that  $G_t$  always has a density denoted by  $\psi_t$  for  $t \in [t_0, T]$ .

From the definition of  $\phi_t^\alpha(h)$ , we can verify that

$$\begin{aligned} & \partial_t \phi_t^\alpha(h) \\ &= \text{div} \left\{ [\log \alpha_t]^\circ \circ \left[ \int_{\mathcal{R}^d} \epsilon \rho_{\beta_t}(h - \alpha_t \circ \epsilon) \mu(d\epsilon) - h \phi_t^\alpha(h) \right] \right\} \\ &= \text{div} \left\{ [\log \alpha_t]^\circ \circ \left[ \mathbb{E}_{\epsilon \sim \mu} \epsilon \rho_{\beta_t}(h - \alpha_t \circ \epsilon) - h \phi_t^\alpha(h) \right] \right\} \\ &= \text{div} \left\{ [\log \alpha_t]^\circ \circ \phi_t^\alpha(h) (\mathcal{D}_t^\alpha(h) - h) \right\}. \end{aligned} \quad (21)$$

Further considering the definition of  $b_t^\alpha(g)$ , we have

$$\text{div}[b_t^\alpha(g) \phi_{T-t}^\alpha(g)] = \partial_t \phi_{T-t}^\alpha(g) \quad (22)$$

Thus, for any  $f \in C_b^1(\mathcal{R}^d)$ , we have

$$f(G_t) = f(G_{t_0}) + \int_{t_0}^t b_s^\alpha(G_s) \cdot \nabla f(G_s) ds. \quad (23)$$

Taking expectations on both sides,

$$\begin{aligned} & \int_{\mathcal{R}^d} f(g) \psi_t^\alpha(g) dg \\ &= \int_{\mathcal{R}^d} f(g) \psi_{t_0}^\alpha(g) dg + \int_{\mathcal{R}^d} \int_{t_0}^t (b_s^\alpha(g) \circ \psi_{t_0}^\alpha(g)) \cdot \nabla f(g) ds dg \\ &= \int_{\mathcal{R}^d} f(g) \psi_{t_0}^\alpha(g) dg - \int_{\mathcal{R}^d} \int_{t_0}^t f(g) \text{div}(b_s^\alpha(g) \psi_{t_0}^\alpha(g)) ds dg. \end{aligned} \quad (24)$$

From the arbitrariness of  $f$ , we know

$$\psi_t(g) = \psi_{t_0}(g) - \int_{t_0}^t \text{div}(b_s^\alpha(g) \psi_{t_0}(g)) ds. \quad (25)$$

Recalling (22) and defining  $\varphi_t^\alpha(g) := \phi_{T-t}^\alpha(g) - \psi_t^\alpha(g)$ , we further have

$$\varphi_t(g) = - \int_{t_0}^t \text{div}(b_s^\alpha(g) \varphi_{t_0}(g)) ds, \quad (26)$$

which holds because  $\psi_{t_0}^\alpha(g) = \phi_{T-t_0}^\alpha(g)$ .

Thus, by the integration by parts, we can obtain

$$\begin{aligned} \partial_t \int_{\mathcal{R}^d} |\varphi_t(g)|^2 dg &= -2 \int_{\mathcal{R}^d} \text{div}[b_t^\alpha(g) \varphi_t(g)] \varphi_t(g) dg \\ &= 2 \int_{\mathcal{R}^d} \varphi_t(g) [b_t^\alpha(g)]^T \nabla \varphi_t(g) dg \\ &= \int_{\mathcal{R}^d} [b_t^\alpha(g)]^T \nabla |\varphi_t(g)|^2 dg \\ &= - \int_{\mathcal{R}^d} \text{div}[b_t^\alpha(g)] |\varphi_t(g)|^2 dg. \end{aligned} \quad (27)$$

Since  $\mathcal{D}_t^\alpha$  is Lipschitz continuous and follows the linear growth condition,  $\text{div}[b_t^\alpha(g)]$  is also bounded. Thus, there exists a finite constant  $C$  such that

$$\partial_t \int_{\mathcal{R}^d} |\varphi_t(g)|^2 dg \leq C \int_{\mathcal{R}^d} |\varphi_t(g)|^2 dg. \quad (28)$$

Since  $\varphi_{t_0}(g) = 0$ , from Grönwall's inequality, we know  $\varphi_t(g) = 0$  for all  $t \in [t_0, T]$ , which is equivalent to (7).

## REFERENCES

- [1] J. Ho, A. Jain, and P. Abbeel, "Denoising diffusion probabilistic models," in *Proc. 34th Int. Conf. Neural Inform. Process. Syst. (NeurIPS)*, Red Hook, NY, USA, 2020, pp. 1–12.
- [2] J. Song, C. Meng, and S. Ermon, "Denoising diffusion implicit models," *arXiv preprint arXiv:2010.02502*, 2020.
- [3] X. Xu, Z. Wang, G. Zhang, *et al.*, "Versatile diffusion: Text, images and variations all in one diffusion model," in *Proc. IEEE/CVF Int. Conf. Comput. Vis. (ICCV)*, 2023, pp. 7754–7765.
- [4] K. Qiu, S. Bakirtzis, I. Wassell, *et al.*, "IRDM: A generative diffusion model for indoor radio map interpolation," in *IEEE Global Commun. Conf. (GlobeCom)*, IEEE, 2023, pp. 01–06.
- [5] G. Chi, Z. Yang, C. Wu, *et al.*, "RF-Diffusion: Radio signal generation via time-frequency diffusion," in *Proc. 30th Annu. Int. Conf. Mobile Comput. Netw. (MobiCom)*, 2024, pp. 77–92.
- [6] B. Fesl, M. Baur, F. Strasser, *et al.*, "Diffusion-based generative prior for low-complexity MIMO channel estimation," *IEEE Wireless Commun. Lett.*, vol. 13, no. 12, pp. 3493–3497, Dec. 2024, ISSN: 2162-2345. DOI: 10.1109/LWC.2024.3474570.
- [7] M. Arvinte and J. I. Tamir, "MIMO channel estimation using score-based generative models," *IEEE Trans. Wireless Commun.*, vol. 22, no. 6, pp. 3698–3713, Jun. 2023, ISSN: 1558-2248. DOI: 10.1109/TWC.2022.3220784.
- [8] L. Yang, Z. Zhang, Y. Song, *et al.*, "Diffusion models: A comprehensive survey of methods and applications," *ACM Comput. Surv.*, vol. 56, no. 4, pp. 1–39, 2023.
- [9] M. Chen, S. Mei, J. Fan, *et al.*, "An overview of diffusion models: Applications, guided generation, statistical rates and optimization," *arXiv preprint arXiv:2404.07771*, 2024.
- [10] A. Lugmayr, M. Danelljan, A. Romero, *et al.*, "Repaint: Inpainting using denoising diffusion probabilistic models," in *Proc. IEEE/CVF Conf. Comput. Vis. Pattern Recognit. (CVPR)*, 2022, pp. 11 461–11 471.
- [11] C. Corneanu, R. Gadde, and A. M. Martinez, "Latentpaint: Image inpainting in latent space with diffusion models," in *Proc. IEEE/CVF Winter Conf. Appl. Comput. Vis. (WACV)*, 2024, pp. 4334–4343.
- [12] A. Liu, M. Niepert, and G. V. d. Broeck, "Image inpainting via tractable steering of diffusion models," *arXiv preprint arXiv:2401.03349*, 2023.
- [13] B. Kawar, S. Zada, O. Lang, *et al.*, "Imagic: Text-based real image editing with diffusion models," in *Proc. IEEE/CVF Conf. Comput. Vis. Pattern Recognit. (CVPR)*, 2023, pp. 6007–6017.
- [14] Y. Huang, J. Huang, Y. Liu, *et al.*, "Diffusion model-based image editing: A survey," *IEEE Trans. Pattern Anal. Mach. Intell.*, 2025.
- [15] Y. Zhang, N. Huang, F. Tang, *et al.*, "Inversion-based style transfer with diffusion models," in *Proc. IEEE/CVF Conf. Comput. Vis. Pattern Recognit. (CVPR)*, 2023, pp. 10 146–10 156.
- [16] R. Sortino, T. Cecconello, A. DeMarco, *et al.*, "RADiff: Controllable diffusion models for radio astronomical maps generation," *IEEE Trans. Artif. Intell.*, 2024.
- [17] X. Luo, L. Zhizhen, Z. Peng, *et al.*, "RM-Gen: Conditional diffusion model-based radio map generation for wireless networks," in *IFIP Networking Conference (IFIP Networking)*, IEEE, 2024, pp. 543–548.
- [18] X. Wang, K. Tao, N. Cheng, *et al.*, "RadioDiff: An effective generative diffusion model for sampling-free dynamic radio map construction," *IEEE Trans. Cogn. Commun. Netw.*, 2024.
- [19] T. O'Shea and J. Hoydis, "An introduction to deep learning for the physical layer," *IEEE Trans. Cogn. Commun. Netw.*, vol. 3, no. 4, pp. 563–575, 2017. DOI: 10.1109/TCCN.2017.2758370.
- [20] R. Sun, N. Cheng, C. Li, *et al.*, "A comprehensive survey of knowledge-driven deep learning for intelligent wireless network optimization in 6G," *IEEE Commun. Surv. Tutor.*, pp. 1–1, 2025. DOI: 10.1109/COMST.2025.3574765.
- [21] F. Zhu, X. Wang, X. Li, *et al.*, *Wireless large AI model: Shaping the AI-native future of 6G and beyond*, 2025. arXiv: 2504.14653. [Online]. Available: <https://arxiv.org/abs/2504.14653>.
- [22] E. Balevi, A. Doshi, A. Jalal, *et al.*, "High dimensional channel estimation using deep generative networks," *IEEE J. Sel. Areas Commun.*, vol. 39, no. 1, pp. 18–30, 2020.
- [23] X. Ma, Y. Xin, Y. Ren, *et al.*, "Diffusion model based channel estimation," in *IEEE Int. Conf. Commun. (ICC Workshops)*, Jun. 2024, pp. 1159–1164. DOI: 10.1109/ICCWorkshops5955.1.2024.10615282.
- [24] N. Zilberstein, A. Swami, and S. Segarra, "Joint channel estimation and data detection in massive MIMO systems based on diffusion models," in *IEEE Int. Conf. Acoust., Speech, Signal Process. (ICASSP)*, Apr. 2024, pp. 13 291–13 295. DOI: 10.1109/ICASSP48485.2024.10446413.
- [25] Y. Yang, O. Alhussein, A. Arani, *et al.*, "Generative diffusion receivers: Achieving pilot-efficient MIMO-OFDM communications," *arXiv preprint arXiv:2506.18419*, 2025.
- [26] Z. Chen, Z. Zhang, Z. Yang, *et al.*, "Channel mapping based on interleaved learning with complex-domain MLP-Mixer," *IEEE Wireless Commun. Lett.*, vol. 13, no. 5, pp. 1369–1373, 2024.
- [27] A. Q. Nichol and P. Dhariwal, "Improved denoising diffusion probabilistic models," in *Proc. Int. Conf. Mach. Learn. (ICML)*, PMLR, 2021, pp. 8162–8171.
- [28] T. Salimans and J. Ho, "Progressive distillation for fast sampling of diffusion models," in *Proc. Int. Conf. Neural Inform. Process. Syst. (NeurIPS)*, vol. 35, Curran Associates, Inc., 2022, pp. 17 870–17 881.
- [29] Y. Yang, Z. Zhang, Z. Chen, *et al.*, "A hybrid inference architecture incorporating neural network with belief propagation for AI receivers," *IEEE Trans. Wireless Commun.*, 2025, Early Access. DOI: 10.1109/TWC.2025.3552818.
- [30] A. Alkhateeb, "DeepMIMO: A generic deep learning dataset for millimeter wave and massive MIMO applications," *arXiv preprint arXiv:1902.06435*, 2019.
- [31] X. Zhang, "New algorithms for sampling and diffusion models," *arXiv preprint arXiv:2406.09665*, 2024.